Supporting Information for

Title: Myosin lever arm directs collective motion on cellular actin network

Author affiliation:

Rizal F. Hariadi[a], Mario Cale[b], and Sivaraj Sivaramakrishnan[a,b,c]
[a]Department of Cell and Developmental Biology,
[b]Department of Biohysics,
[c]Department of Biomedical Engineering,
University of Michigan, Ann Arbor, Michigan 48109, USA

Corresponding author

Sivaraj Sivaramakrishnan
3045 BSRB,
109 Zina Pitcher Place,
Ann Arbor, MI 48109-2200, USA
Ph: 734-764-2493
Fax: 734-763-1166
e-mail: sivaraj@umich.edu

This PDF file includes

Supplemental Methods
Supplemental Figures S1–S14
Legends for Supplemental Movies S1–S2
Supplemental Notes S1
Supplemental Table S1

Supplemental Methods

Buffer and reagents – 1X Assay Buffer (AB) - 25 mM imidazole (pH 7.5), 4 mM $MgCl_2$, 1 mM EGTA, 25 mM KCl, 10 mM DTT; 1X AB.BSA buffer, AB buffer + 1 mg/mL BSA.

Preparation of benzyl-guanine-conjugated oligo – C6-amine modified oligonucleotides (oligo) were covalently linked to benzyl-guanine NHS-ester (BG-GLA-NHS; NEB). Briefly, 0.08 mM oligo was incubated with 3.2 mM BG-GLA-NHS in 0.1M $NaBO_3$ for ~8 hr at room temperature with shaking. Oligo was precipitated in a final concentration of 70% ice-cold ethanol followed by multiple washes and centrifugation (12,000g; 30 min) steps to remove unreacted BG-GLA-NHS. Air-dried pellet was reconstituted in 2 mM Tris pH 8.5 followed by desalting (2x) on G-50 MicroColumns (GE Healthcare). Final benzyl-guanine labeled oligo (BG-oligo) concentration was determined from UV absorbance at 260 nm (Nanodrop). BG oligo aliquots were frozen and stored at -80 °C.

Covalent oligo attachment to myosin protein – Myosin protein bound to Anti-FLAG resin was incubated with excess (>10 μM) of benzyl-guanine-conjugated oligo (BG-oligo) at 37 °C with shaking for 30 min followed by overnight incubation on ice. Resin was washed 3 times with buffer containing 20 mM Imidazole pH 7.4, 3 mM DTT, 1 μg/ml PMSF, 10 μg/ml aprotinin, and 10 μg/ml leupeptin. BG-oligo labeled myosin was eluted with 0.2 mg/ml FLAG-peptide (Sigma) and was used within two weeks or stored in a 55% v/v glycerol solution at –20 °C. Labeling efficiency was assessed by separating labeled and unlabeled myosin by 10% SDS-PAGE followed by staining with SimplyBlue SafeStain (Invitrogen). Myosin labeled with BG-oligo showed a distinct gel-shift with over 95% labeling efficiency quantified by densitometry.

Origami preparation and purification – DNA sequences are listed in the SI Notes 1. Three strands are used in tandem to enable purification of scaffold-myosin complexes by strand displacement (Fig. S5). The origami-attachment strand is an extended staple strand; the spacer strand has complementarity to the origami-attachment strand; the biotin-strand has complementarity to the spacer strand. Further, staple strands at the sites of myosin attachment have a 5T's extension to provide the bound myosin with rotational freedom. Last, the 23 edge- staple strands were extended with a unique DNA sequence. A single Cy3 DNA strand with complementarity to this edge-staple extension was used to label each scaffold with 23 Cy3 dye molecules. Purified scaffolds were stored at 4 °C.

Scaffold-myosin purification – Affinity purification was achieved with a nitrocellulose coverslip coated with neutravidin. Biotinylated, myosin-scaffold mixtures were bound to the coverslip for 5 min. Subsequently, the coverslips were extensively washed with AB supplemented with 0.1 mg/ml BSA. Myosin scaffolds were eluted with AB.BSA and 9 μM calmodulin. Elution was achieved by competitive displacement of the spacer strand with a highly complementary elution strand (10 min at RT; Fig. S5). Purified myosin-scaffold complexes were immediately used in motility assays. The yield and integrity of scaffold- myosin conjugation was assessed using 1% agarose - 0.1% SDS gels.

SDS-Agarose Gel – The purity, yield, and structural integrity of myosin-origami conjugation was assessed by a gel-shift assay. The myosin-origami samples were incubated with loading dye (Promega) containing 1% SDS for 5 minutes. The samples were loaded onto 1% agarose-0.1% SDS gel and run in 1X TE, 0.1% SDS, and 5 mM $MgCl_2$ for 6-10 hours, at 60 V, at room temperature.

Cy3-myosin conjugation for single molecule experiments – Purified BG-oligo1-labeled myosin dimers were mixed with an excess of Cy3-RC-oligo1-Cy3 strand (5'- Cy3-ACTATAGAGATTGGCGCGTATCGT-Cy3 -3') and incubated in binding buffer (10 mM Imidazole, pH 7.4, 25 mM KCl, 10 mM $MgCl_2$) supplemented with 1 mg/mL BSA and 9 μM calmodulin for 20 minutes at ambient temperature (RC refers to the reverse complement). Cy3-labeled myosin was purified from the excess of Cy3-RColigo1-Cy3 by Nickel-NTA agarose resin (Qiagen). First, the labeled myosin was bound to the resin for 30 minutes on ice. Resin was extensively washed with assay buffer containing 1 mg/mL BSA to remove unbound Cy3-RColigo1-Cy3 strands. The purified Cy3-labeled myosin was eluted from the resin by buffer consisting of 200 mM Imidazole, pH 7.4, 1 mM EGTA, 4 mM $MgCl_2$, 25 mM KCl, 9.0 μM calmodulin, 10 μg/mL Aprotinin, 10 μg/mL Leupeptin, 0.1 mg/mL PMSF, and 10 mM DTT. Potential aggregates were removed by centrifugation for 15 minutes at 21.2×10^3 g on a bench top centrifuge at 4°C.

Preparation of keratocyte actin networks – Keratocytes were derived from scales of *Thorichthys meeki* (Firemouth Cichlids) as previously described (26). All protocols conform to the guidelines of the local animal care and use committee (IACUC). As previously reported (26), keratocytes were detergent-extracted and actin networks were stabilized with phalloidin [50 nM Alexa-488 phalloidin (Invitrogen) with 200 nM unlabeled phalloidin (Sigma)]. Coverslips with detergent extracted keratocytes were stored at 4°C and used in motility experiments within 24 hrs.

Single molecule imaging – Single molecule motility assays were acquired at 240x magnification on an objective-based TIRF microscope (Olympus IX81) with a 60x NA 1.48 Apo TIRF objective (Olympus), 4x image magnifier, EMCCD iXON Ultra, and a 561 nm laser (Coherent, 50 mW max power, 6 mW near objective). Movies of scaffold motility on the keratocyte actin network were obtained at 2 Hz for >20 minutes.

Scaffold-myosin imaging – Motility assays of Cy3-labeled scaffold with myosin motors were imaged at 150x magnification on a Nikon TiE microscope equipped with a 100x 1.4 NA Plan-Apo oil-immersion objective, 1.5x magnifier, a mercury arc lamp, Evolve EM-CCD camera (512 pixel x 512 pixel; Photometrics) and Nikon NIS-Elements software. Movies of myosin-scaffold motility on keratocyte were acquired at 2 Hz for 10–60 minutes per field of view.

Run length and end-to-end speed – Analysis of myosin labeled scaffold movement was restricted to scaffolds that appeared for more than 6 continuous frames (3 sec) and covered a distance of more than 3 pixels (320 nm). Scaffolds that were temporarily stalled were excluded from the run length analysis. Run lengths were measured by fitting a trajectory into linear segments of 300 nm starting with the first appearance of the

scaffold. Run-length distribution was fitted to the truncated cumulative distributive function (CDF) of a single exponential distribution, $CDF(x) = 1\text{-}e^{-(x\text{-}xmin)/\lambda}$, where λ is the mean run length and x_{min} is the *a priori* minimum measurable run length (600 nm). End- to-end speeds were calculated by dividing measured run length (see above) by the total time the scaffold remained bound to the keratocyte network. The run length is reported as mean±SEM of the parameter λ, derived from the fit. The SEM was estimated by the bootstrap method.

Stochastic simulation – Detailed description of the simulation is presented in Fig. S11.

Atomic Force Microscopy imaging – AFM images were acquired using tapping mode on a Nanoscope IIIa (Bruker Corporation). We used a SNL silicon nitride cantilever (Bruker AFM Probes) of length 110 μm and spring constant 0.38 N/m. Samples were imaged in AB with excess myosin and BSA removed by purification with Strepavidin magnetic beads (NEB; S1420S). Briefly, 10 μL of purified sample was deposited on a freshly cleaved piece of mica (Ted Pella), ~ 1 cm × 1 cm in size, affixed to a 15-mm diameter magnetic stainless steel puck (Ted Pella). After the DNA scaffolds are immobilized on the mica, an additional 20 μl of AB was added to both sample and cantilever holder before imaging.

Statistical analysis –The p values were computed by two-tail unpaired Student's t test using Prism 6 data analysis software (GraphPad). All reported measurements are expressed as mean ± standard error of mean (SEM). The bootstrap method was used to estimate the uncertainty (SEM) of a measurement of X from the full data set. Bootstrap method was used to analyze shape factor (*S*; Figs. 1, 3, 4, 5, 6), normalized photon intensity (*I*; Fig. 2), speed (*v*; Figs. 3A and S8), run length (*RL*; Figs. 3B and S9). The analysis was performed with either MATLAB or Mathematica. First, from the full data set of sample size *N*, a subset of size $\lfloor N/2 \rfloor$ was randomly chosen to compute x_j. The brackets denote rounding off to the nearest integer. In a random subset, an element was never chosen more than once. The value of x_j was generated ≥1000 times. As *j* increases, the distribution of x_j approaches a normal distribution $\langle x_j \rangle \rightarrow X$. Finally, the standard deviation of x_j was used as an estimate of the uncertainty in the measurement of X.

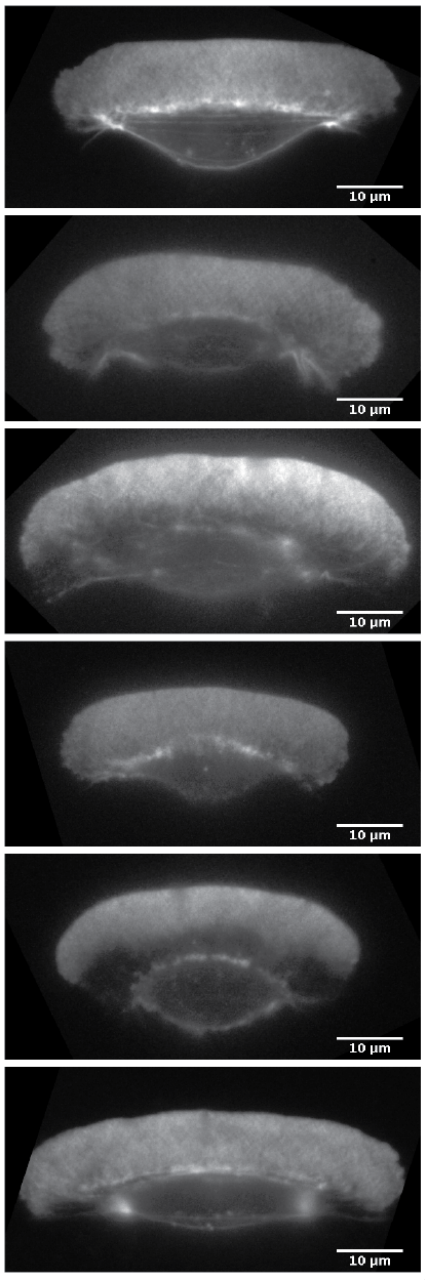

Figure S1 – Sample keratocyte actin networks - Representative fluorescence images of fish epidermal keratocyte networks after detergent extraction. The actin networks were stabilized with a combination of Alexa488-phalloidin and dark-phalloidin (1:4) during the extraction.

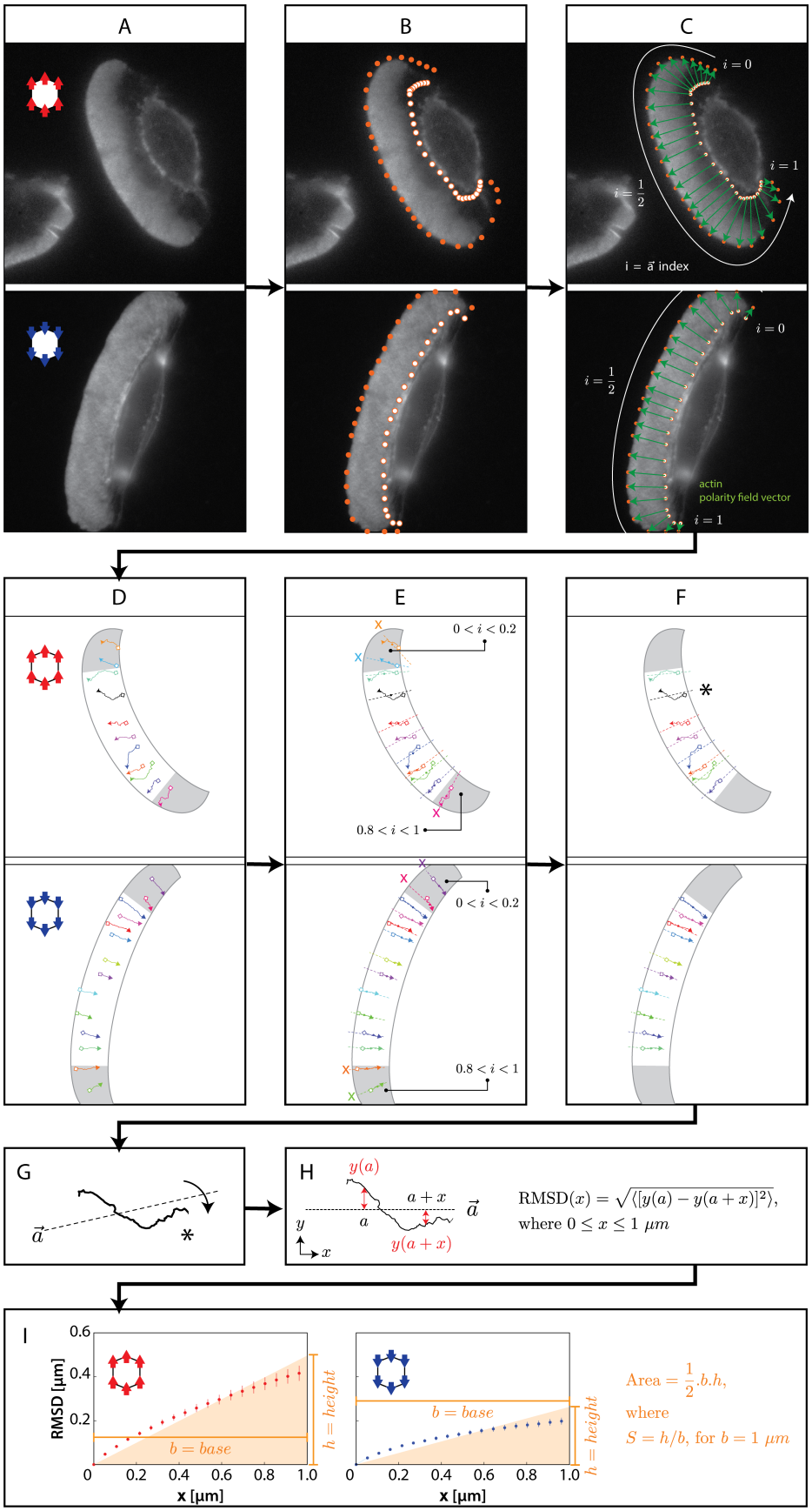
A
B
C
$i = 0$
$i = 1$
$i = \frac{1}{2}$
i = a⃗ index
actin
polarity field vector
D
E
F
$0 < i < 0.2$
$0.8 < i < 1$
G
$\vec{a}$
H
$y(a)$
$a + x$
a
y
x
$y(a + x)$
$\vec{a}$
$\mathrm{RMSD}(x) = \sqrt{\langle [y(a) - y(a+x)]^2 \rangle}$,
where $0 \leq x \leq 1\ \mu m$
I
RMSD [µm]
0.6
0.4
0.2
0
0.2
0.4
0.6
0.8
1.0
x [µm]
$b = base$
$h = height$
$\mathrm{Area} = \frac{1}{2}.b.h,$
where
$S = h/b$, for $b = 1\ \mu m$

Figure S2 (previous page) **– Procedure for calculating the shape factor for a set of trajectories**

(**A**-**F**) Analysis of selected trajectories for scaffolds with either 6 myosin VI (top half) or scaffolds with 6 myosin V (bottom half). These steps were used for computing the shape factor for both experimental and simulated trajectories in Figs. 1, 3, 4, 5, and 6.

(A) Keratocyte image.

(B) Selected coordinates of ≥20 equidistant points near the cell center (open orange circles) and at the cell periphery (closed orange circles).

(C) Vectors connecting points from the cell center to the cell periphery (green arrows) were used to generate a set of actin polarity field vectors across the actin surface. Each vector was given an index $0 \leq i \leq 1$, based on its starting position.

(D) Trajectory coordinates are loaded on to the actin polarity field vector map.

(E) Center of mass $\{x_{CM}, y_{CM}\}$ of each trajectory is calculated as
$x_{CM} = \frac{1}{N}\sum_j^N x_j$ and $y_{CM} = \frac{1}{N}\sum_j^N y_j$
where N is the number of points in a trajectory. A binary search algorithm was used to find an actin polarity field vector (dashed arrows) that passes through $\{x_{CM}, y_{CM}\}$.

(F) Trajectories with index $0 \leq i \leq 0.2$ and $0.8 \leq i \leq 1.0$ were excluded from the data analysis in order to avoid complications due to the possible variation in actin architecture at the keratocyte edges.

(G) The trajectories in (**F**) were rotated to align their local actin polarity field vector to a horizontal axis (x). As an example, the * trajectory in (**F**) was rotated clockwise (**B**). The rotated * trajectory is presented in (**H**).
At this step, aligned trajectories from multiple keratocytes can be combined into a single data set. Examples of ensembles of aligned trajectories are presented in Figs. 1D–E, 3E–F, 5C–D, and 6B–C.

(H) Root mean squared sisplacement (RMSD) was calculated relative to the axis of the local actin polarity field vector ($\vec{a}$). RMSD is defined as
$RMSD(x) = \sqrt{\langle [y(a) - y(a+x)]^2 \rangle}$, where $0 \leq x \leq 1$ μm.

(I) The RMSD(x) was fit to a polynomial of order n (x^n). The area under this curve was calculated by integrating the fitted polynomial from 0–1 μm. The height of a triangle with the same area and a base of 1 μm is defined as the shape factor. Mathematically, the shape factor (S) is expressed as
$A = \frac{1}{2}.b.h$
where A = area of the shaded triangle, b = base, and
h = height. Then, $S = h/b$, for b = 1 μm.

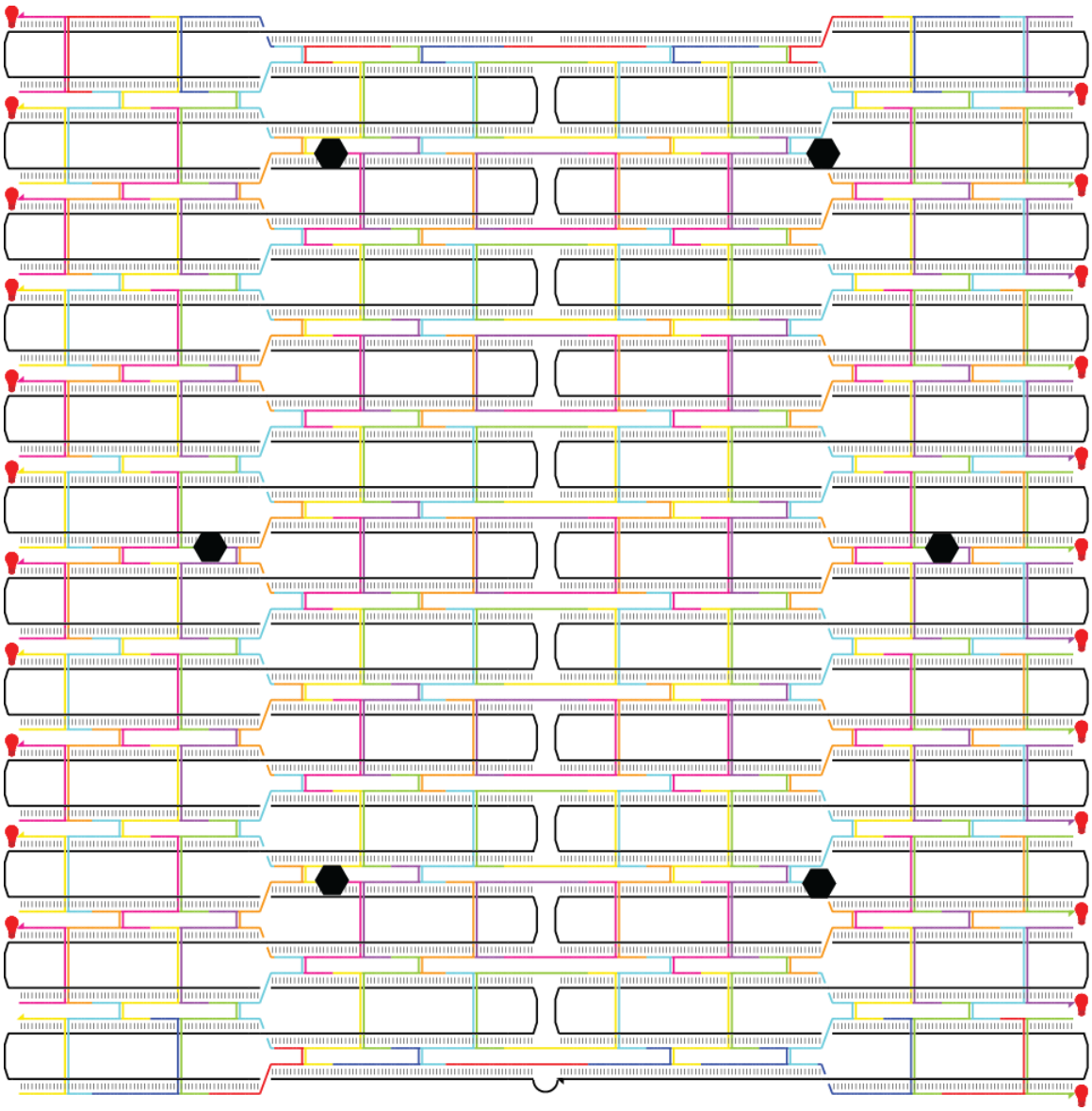

Figure S3 – Flat rectangular DNA origami scaffold design – The main core of the scaffold is a flat rectangular DNA origami with 10.44 bp/turn, consisting of 24 parallel DNA helices *(Woo and Rothemund, Nat. Chem, 2011)*. The scaffold strand is shown as a continuous thick black line. The 6 possible attachment sites for DNA-labeled myosin V or VI are depicted as black hexagons. The bottom left staple strand is extended for affinity-based purification (Fig. S5). With the exception of the edge-staple strand at the bottom left corner, each staple strand is labeled with 23 Cy3 fluorophores (shown as red light bulbs) to facilitate single molecule microscopy and myosin occupancy assays.

Figure S4 - Sequence diagram for a flat rectangular DNA origami scaffold with 10.44 bp/turn *(Woo and Rothemund, Nat. Chem., 2011)* – The scaffold strand is displayed in white.

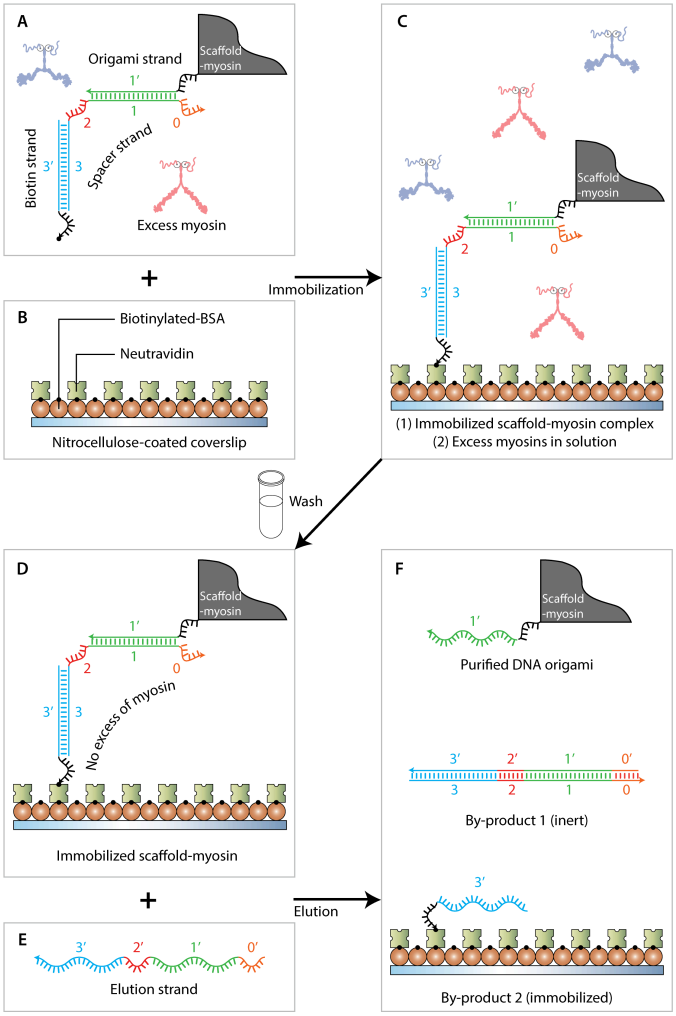

Figure S5 – Purification steps to remove the excess myosin – (**A**) Each scaffold is agarose-purified to remove excess staple strands. The agarose-purified scaffold (gray) contains three short oligos for further purification of scaffold-myosin complexes, namely an origami strand (1'; green), a biotin strand (3'; blue), and a spacer strand (123; green-red-blue). (**B**,**C**) The origami-myosin complexes are immobilized on a neutravidin-coated surface (22x22 mm coverslip) by a BSA-biotin-neutravidin linkage. The unconjugated myosins are free in solution. (**D**) The excess myosin is washed away by a gentle immersion step in a 50 mL Falcon tube filled with AB (see SI Methods) and 0.1 mg/mL BSA. (**E**) An elution strand (0'1'2'3'; orange-green-red-blue) is presented to the immobilized scaffold-myosin complex. (**F**) The elution strand releases the scaffold-myosin complex into solution by a branch migration reaction, while releasing the inert elution-spacer complex as a by-product. Purified myosin-scaffold complexes are immediately used in motility assays.

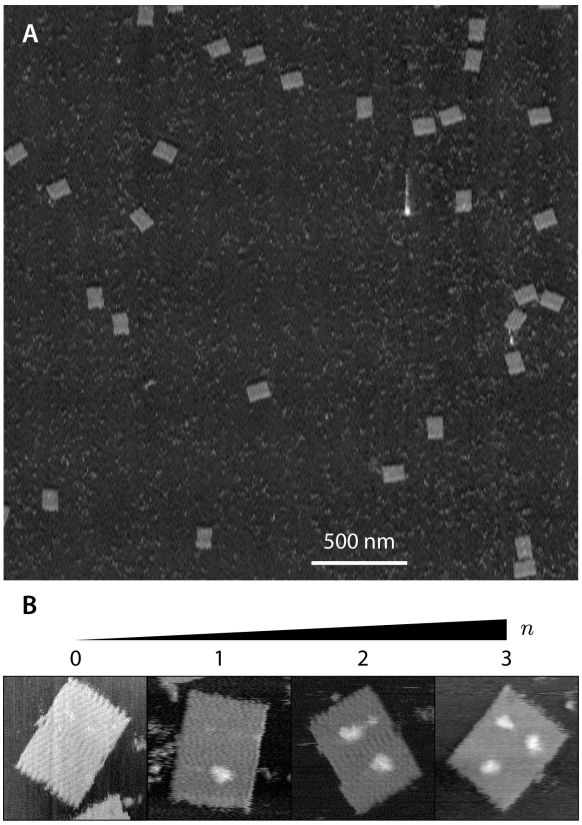

Figure S6 – AFM images of purified DNA scaffolds – (**A**) Representative AFM image of purified DNA scaffolds showing the structural integrity (> 95%) after the purification step (Fig. S5). (**B**) High resolution AFM images of DNA scaffolds with n = 0, 1, 2, and 3 myosin V motors. The size of the DNA scaffold is ~100 nm x 80 nm.

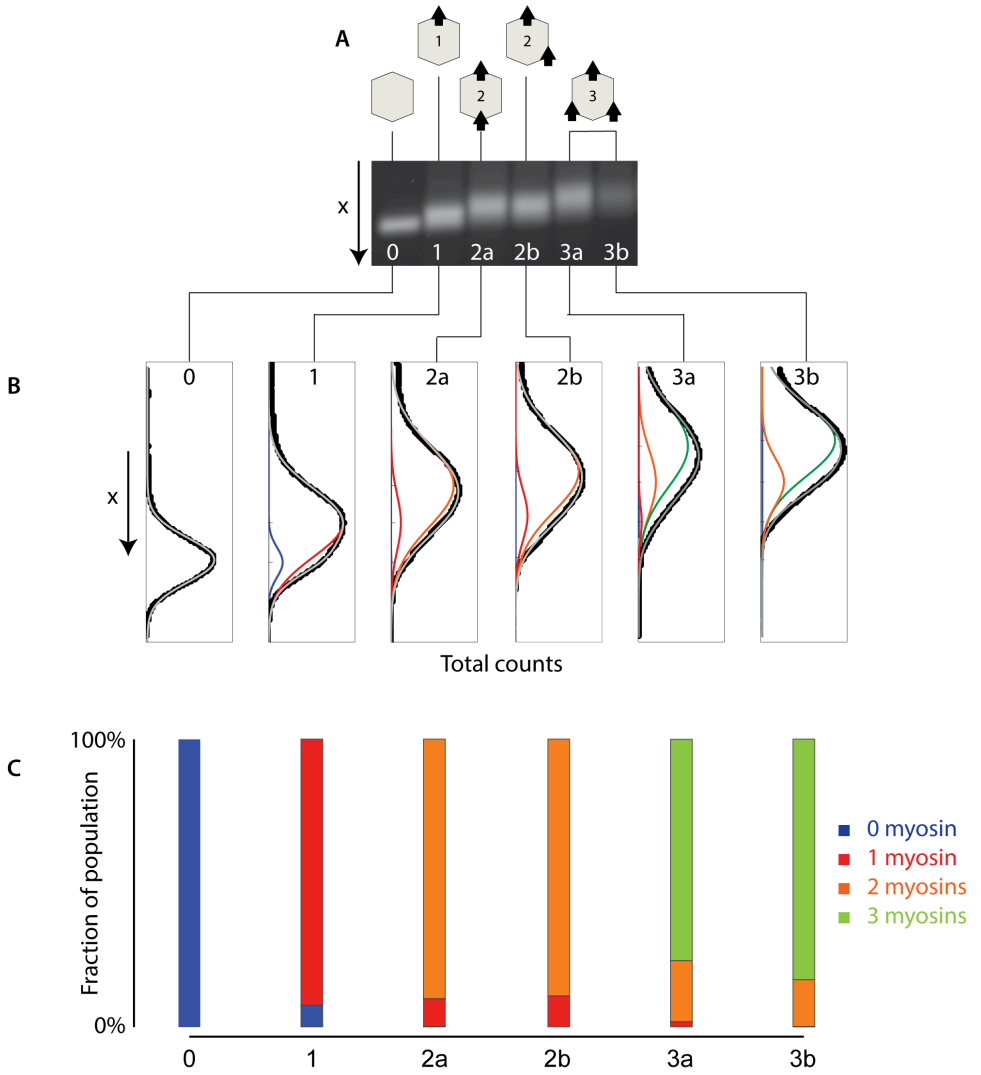

Figure S7 – Quantifying myosin occupancy based on agarose gel shift – (**A**) SDS-agarose gel shift of Cy3-labeled scaffolds with 0, 1, 2, and 3 DNA binding strands in the presence of DNA-myosin complexes. The gel is a duplicate image of Fig. 2D of main text. (**B**) Myosin occupancy was estimated by fitting the intensity profile of each band along the electrophoresis direction (black dots). The intensity profile for each condition is derived from a summation of profiles for distinct myosin occupancies, each of which is assumed to be Gaussian distributed. Thus the intensity profile in each lane is the sum of Gaussians corresponding to 0 (blue), 1 (red), 2 (orange) and, 3 (green) myosins each of which has a distinct mean location along the gel, amplitude, and standard deviation. The observed intensity profiles were iteratively fit to the sum of Gaussians. The fraction of population of scaffolds with *n* myosin was calculated from the area under corresponding Gaussian curve. In our analysis, we assume that each myosin-binding process is an independent event. For each binding site, myosin occupancy (O) is defined as the probability of binding. Global fitting of the different conditions to a binomial distribution yielded a myosin occupancy of 0.94±0.1. (**C**) Calculated stacked histograms of the population distribution for each condition. The analysis was limited to scaffolds with 3 myosins due to the large number of free parameters in the fitting step. The high myosin occupancy is consistent with similar values estimated from the photon counting assays (O = 0.92–0.97; Figs. 2E–G).

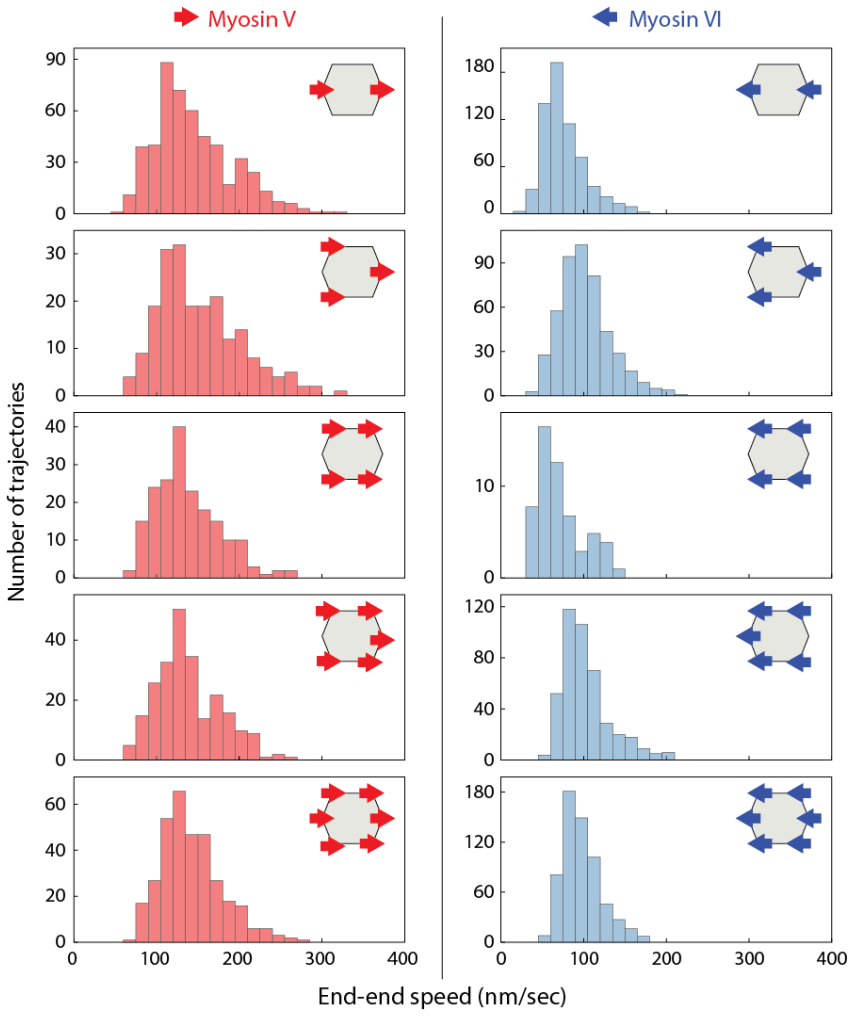

Figure S8 – End-to-end speed distributions for scaffolds with either myosin V or VI – Histograms of end-end speed for the indicated configuration (upper right corner of each histogram) of myosin V (red; left panels) or myosin VI (blue; right panels). Short trajectories (RL<1 μm) are excluded from the data analysis. For either motor type the collective speed does not depend on multi-motor number (P<0.002, $N_V \geq 71$, $N_{VI} \geq 58$). Myosin V scaffolds (regardless of motor number) move significantly faster than those with myosin VI (P <0.01, $N \geq 58$).

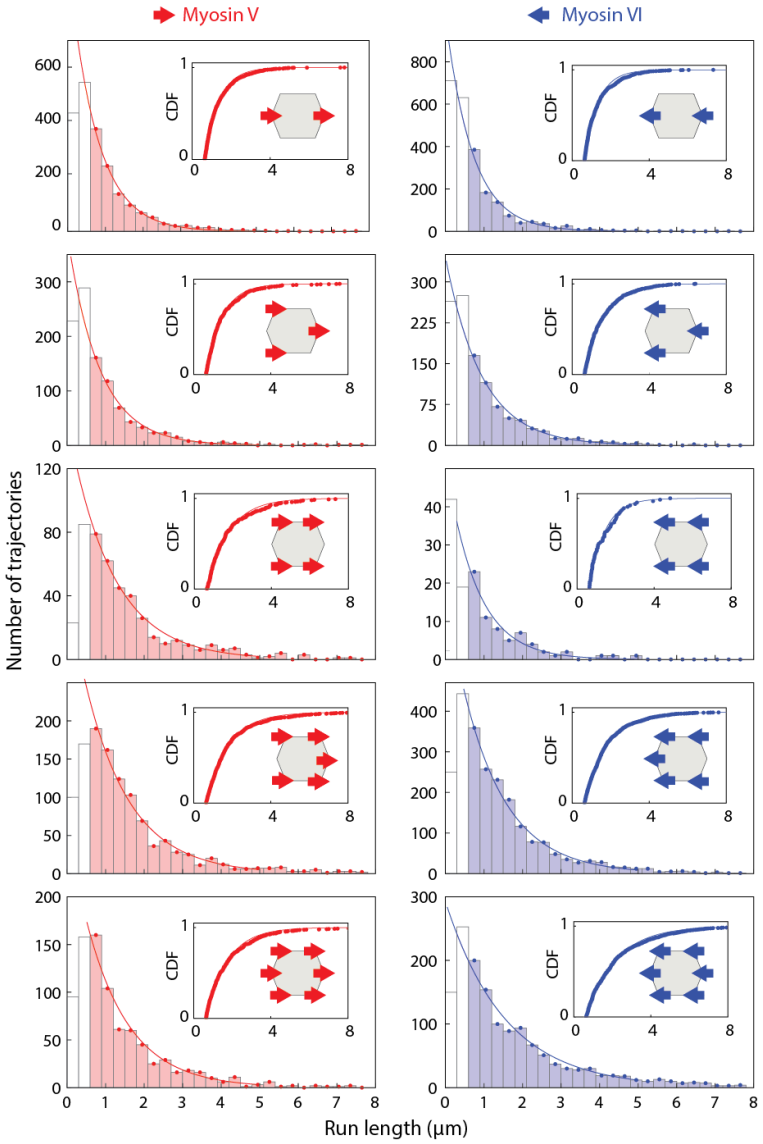

Figure S9 – Run length distribution for scaffolds with multiple myosin V or VI – Run length histograms of scaffolds with myosin V (red; left panels) or myosin VI (blue; right panels). The number and configuration of myosin V (red) and myosin VI (blue) are shown in the insets. Solid lines are single exponential fits based on the cumulative distributive functions (CDF; insets), with a minimum measurable run length (threshold) of 600 nm. The white bars are runs shorter than 600 nm (the number of short runs is an underestimate as they are limited by the spatial and temporal resolution of our image acquisition). For both myosin types, the run length increases with motor number and is summarized in Fig. 3B of the main text.

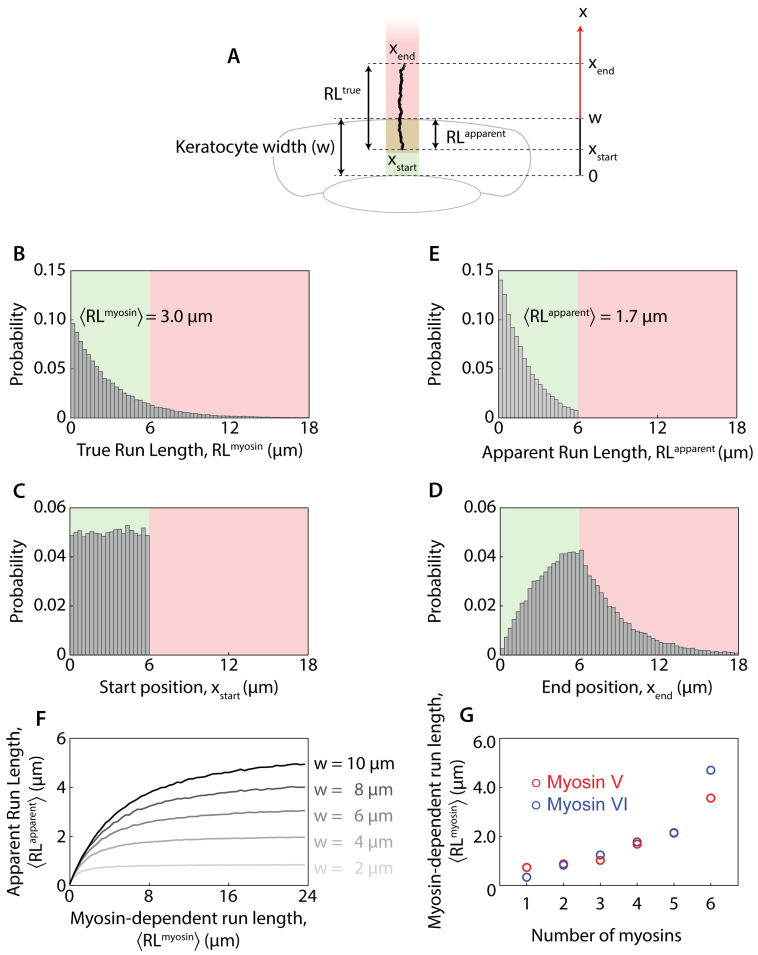

Figure S10 – The measured run length is limited by the finite width of the keratocyte actin network – **(A)** Model for scaffold movement on an infinitely long one-dimensional track. On keratocytes, the track is limited by the keratocyte width w, which is displayed as the green-shaded region in all panels. Scaffolds that enter the red-shaded region are truncated at the keratocyte boundary x=w. **(B)** On an infinitely long track, the distribution of myosin-dependent run lengths (RL_i^{myosin}) follows a single exponential distribution. **(B-E)** The relationship between myosin-dependent and observed (apparent) run lengths is illustrated with w = 6 µm and $\langle RL^{myosin} \rangle$ = 3 µm. **(C)** The start position x_i^{start} of trajectory i is uniformly distributed between 0 and w. **(D)** Trajectory i dissociates from the track at $x_i^{end} = x_i^{start} + RL_i^{myosin}$. Due to the limited keratocyte width, trajectories that travel beyond the keratocyte periphery get truncated at $x = w$. Based on this model, the limited track length preferentially truncates long trajectories. **(E)** As a consequence, the mean apparent run length $\langle RL^{apparent} \rangle$ is calculated to be 1.7 µm, well below $\langle RL^{myosin} \rangle$ = 3.0 µm. **(F)** The mean apparent run length of scaffold-motor complexes with $0<\langle RL^{myosin} \rangle<24$ µm on a keratocyte track of width w = 2, 4, 6, 8, and 10 µm. Based on the model, the limit of mean apparent run length $\langle RL^{apparent} \rangle$ on a keratocyte track of width w is $w/2$. **(G)** Estimated myosin-dependent run lengths for average keratocyte width (w) of 6 µm.

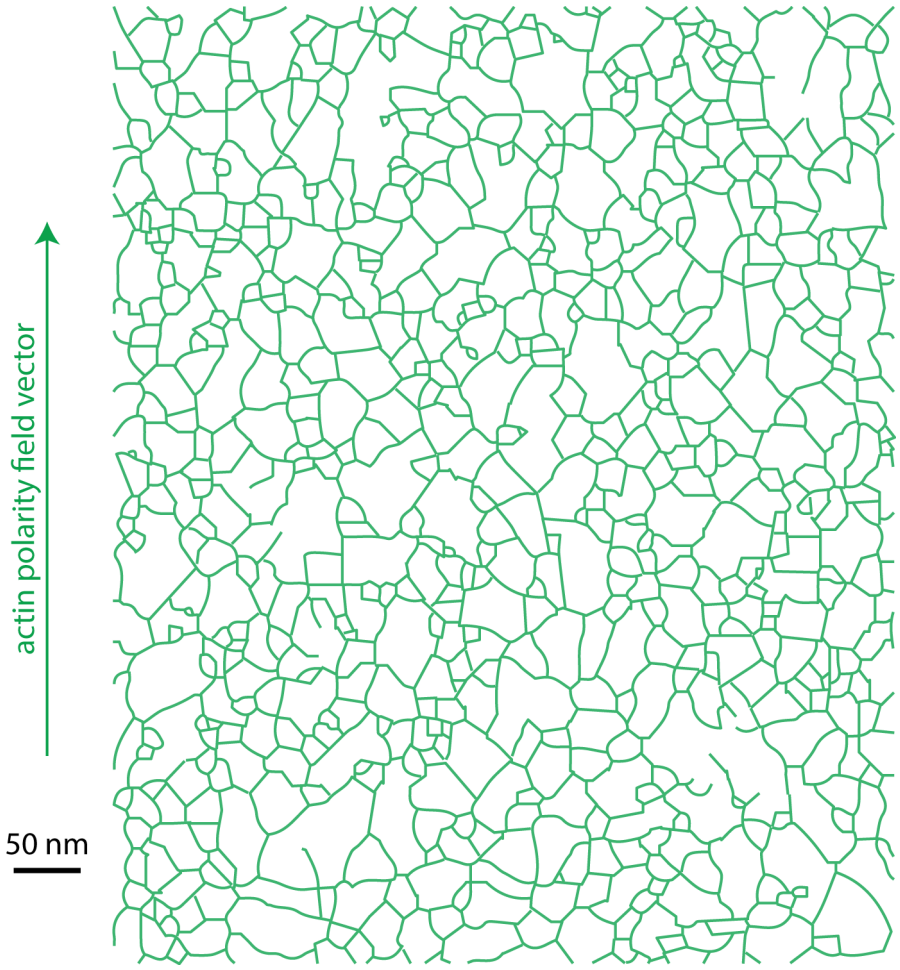

Figure S11 – Skeletonized TEM image of the interlaced actin network used in the stochastic simulation (Fig. S12). The actin polarity field vector (green arrow) points upward. Given that the pore size of the meshwork (~30 nm; *Sivaramakrishnan and Spudich, J. Cell. Biol, 2009*) is substantially smaller than that of the origami scaffold, this analysis is restricted to filaments located near the keratocyte surface with depth information derived from the intensity of the platinum replica micrographs (see Methods).

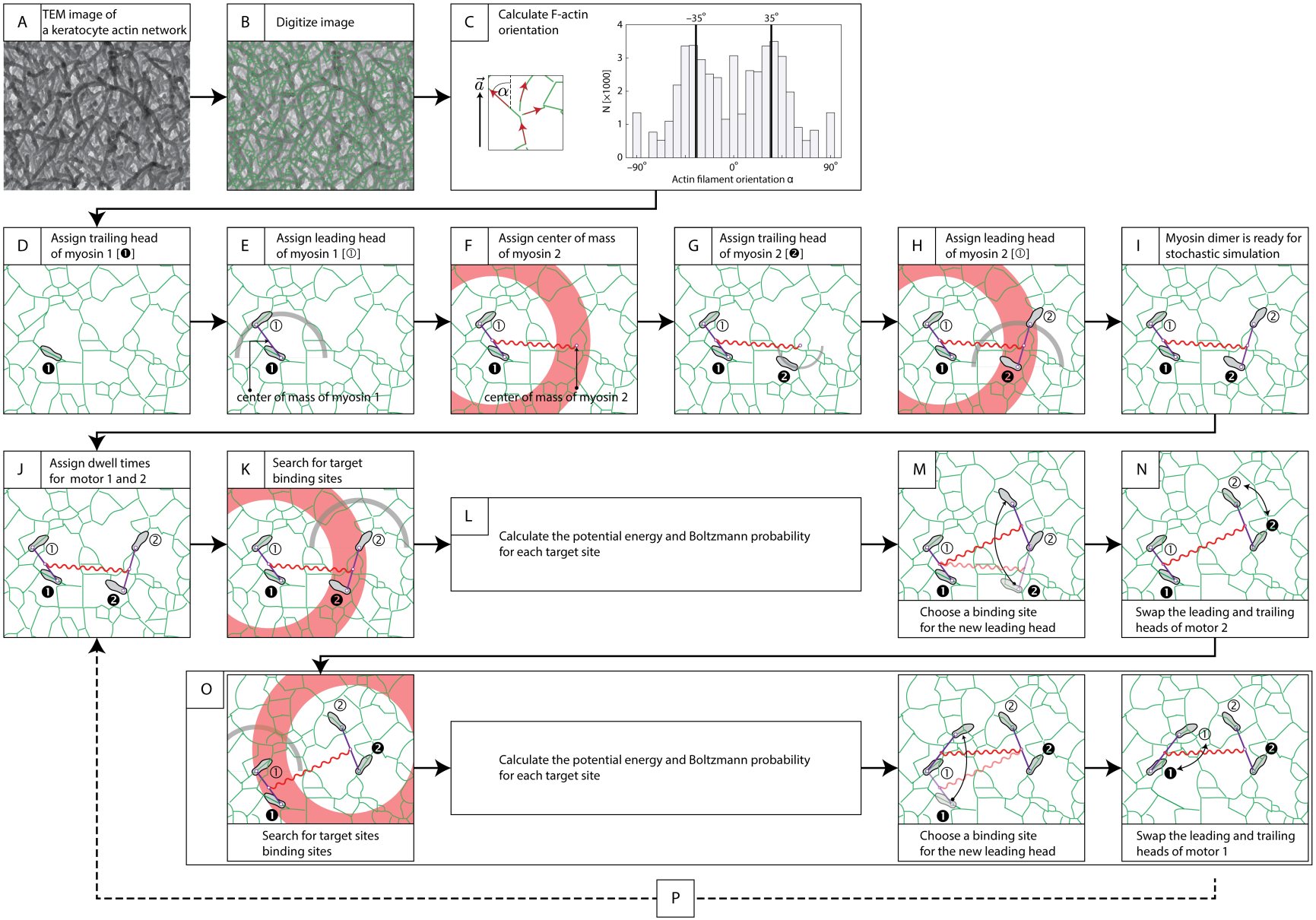
A
TEM image of
a keratocyte actin network
B
Digitize image
C
Calculate F-actin
orientation
$\vec{a}$
α
−35°
35°
N [×1000]
0
1
2
3
4
−90°
0°
90°
Actin filament orientation α
D
Assign trailing head
of myosin 1 [❶]
E
Assign leading head
of myosin 1 [①]
center of mass of myosin 1
F
Assign center of mass
of myosin 2
center of mass of myosin 2
G
Assign trailing head
of myosin 2 [❷]
H
Assign leading head
of myosin 2 [①]
I
Myosin dimer is ready for
stochastic simulation
J
Assign dwell times
for motor 1 and 2
K
Search for target
binding sites
L
Calculate the potential energy and Boltzmann probability
for each target site
M
Choose a binding site
for the new leading head
N
Swap the leading and trailing
heads of motor 2
O
Search for target sites
binding sites
Calculate the potential energy and Boltzmann probability
for each target site
Choose a binding site
for the new leading head
Swap the leading and trailing
heads of motor 1
P

Figure S12 (previous page) – **Description of stochastic simulation** –

Stochastic simulations of myosin-scaffold movement on the digitized actin network were performed using a custom MATLAB code based on the rules described below.

(A) Platinum replica micrograph image of a keratocyte actin network. This image is used to simulate long movement trajectories using periodic boundary conditions.

(B) The position of actin filaments (green lines) was derived from the digitized image of actin network in (**A**) as described in *Sivaramakrishnan and Spudich, J. Cell. Biol, 2009*. Each pixel is a possible microstate for the myosin head.

(C) For every pixel in the skeletonized image, we calculate the orientation of the actin filament relative to the actin polarity field vector. A 7x7 search box, centered on each actin filament pixel is fitted to a linear function. The local actin filament direction is the inverse tangent (*arctan*) of the slope of the fit line. Actin pixels with low goodness of fits (R^2<0.25, 14% of the detected pixels in (**B**)) were excluded from the simulation in order to exclude multi-filament junctions. The local filament directions are stored in order to calculate microstate energies bed in step (**L**).

In our model, a myosin dimer consists of 2 identical myosins with lever arm stiffness k_f (Fig. 4B) or 2 unique myosins with lever arm stiffness k_{f1} and k_{f2} (Fig. 6E). The centers of mass of myosin 1 and 2 are linked by a linear spring k_s. Each myosin motor comprises 2 motor domains (gray sandals). Each myosin has a leading (① or ②) and trailing head (❶ or ❷).

(D) The trailing head of motor 1 is positioned randomly on an actin filament.

(**E**–**H**) The position of the leading head (**E**) and the second myosin (**F**–**H**) are randomly assigned such that the distance between the heads is 36± 4 nm (gray arc; (**E** and **H**)) and the centers of mass of the two motors are within 65±15 nm (red ring; (**F** and **H**)).

(I) At each simulation step, we keep track the position of 4 myosin heads, 2 centers of mass, and the center of the two centers of mass.

(J) Myosin dimers step stochastically with an exponentially distributed dwell time on the actin filament. Hence, the dwell times for each step are derived from an exponential distribition of mean dwell times based on the cycle rates of myosin V and VI [*De La Cruz et al., PNAS 1999*; *De La Cruz et al, J. Biol. Cell. 2001*]. The myosin with the shortest dwell takes the first step. For illustration purpose, $t_1 > t_2$, and myosin 2 moves first.

(K) The trailing head pivots about the lead head. The next binding site is determined by the following criteria:

a. within 36± 4 nm pixel from the leading head (gray arc),
b. the new center of mass is within 65±15 nm (red ring) from the center of mass of the other motor (myosin 1), and
c. myosins proceed in forward direction based on the polarity of the actin network.

(L) We calculate the energy and Boltzmann probability (Fig. 4B) for each selected pixel.

(M) Based on the Boltzmann probability of each pixel, we stochastically choose the binding site for the new leading head.

(N) The old leading head is now assigned as the new trailing head and the coordinates of the centers of mass are reassigned.

(**O**–**P**) The process is repeated for the other myosin (**J**–**N**) followed by repetitions of (**J**–**O**) to generate trajectories.

For each condition, the simulation was repeated for ≥ 4 times. Simulated trajectory shapes were quantified in terms of shape factor (Fig. S2). To construct the shape factor plots in Figs. 4, S13, and S14, the mean shape factors were fitted to a sigmoidal function (solid lines in Figs. 4 and S14; dashed line in Fig. S13) below:

$S(x) = S_o + a\ \frac{1}{1+e^{-(x-x_o)}}$, where S_o, a, x_o are the fitting parameters and $x = 10^{k_s/k_s}$.

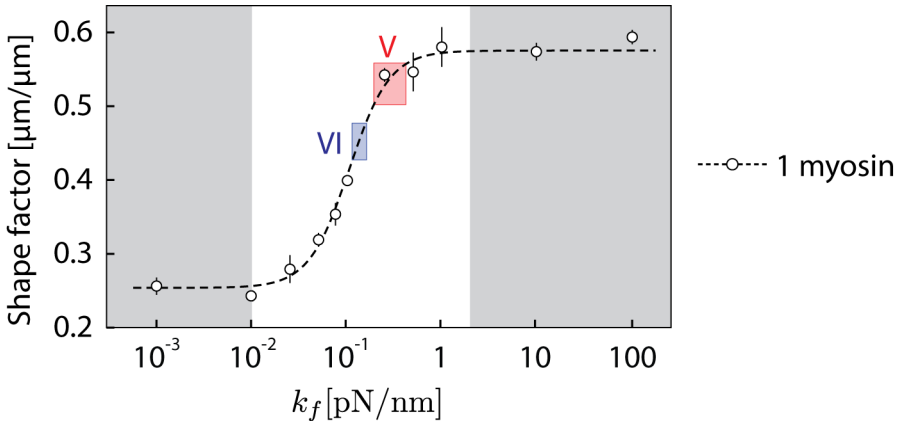

Figure S13 – Lever arm rigidity controls the trajectory shapes for single myosins – Shape factor of simulated trajectories is influenced by the lever arm stiffness k_f. Therefore, the rigidity of the lever arm can be tuned to match the observed trajectory shapes in Fig. 1 of the main text. The experimentally measured shape factors for single myosin V (red-shaded box) or myosin VI (blue-shaded box) were used to calculate corresponding lever rigidities (k_f) of 0.30±0.18 pN/nm and 0.16±0.02 pN/nm, respectively. Movement trajectories of single myosins with either thermally flexible ($k_f L^2 < k_B T$) or rigid ($k_f L^2 >> k_B T$) lever arms are insensitive to k_f (gray-shaded regions).

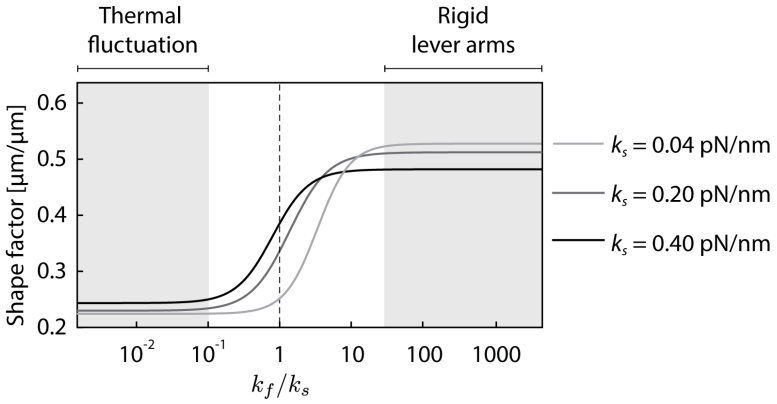

Figure S14 – Shape factors for simulated trajectories of scaffolds with 2 myosin motors connected by an inter-motor spring with stiffness (k_s) = 0.04, 0.20, and 0.40 pN/nm. Sigmoidal lines are derived from simulations with varying k_f / k_s for indicated k_s values. These simulations support k_f / k_s as the primary determinant of trajectory shape factor. Data presented in the main text are for k_s = 0.20 pN/nm. Gray regions indicate regimes dominated by thermal fluctuation or rigid lever arms.

Legends for Movies S1 and S2

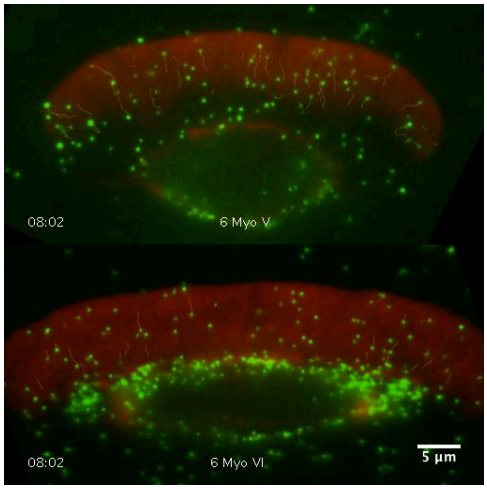

Movie S1 – (**top**) Movie of scaffolds with 6 myosin V (green) meandering on a keratocyte actin network (red) (Fig. 3C). (**bottom**) Scaffolds with 6 myosin VI (green) moving linearly on the two-dimensional network (Fig. 3D). Data was acquired at 2 Hz frame rate, 2 mM ATP, RT.

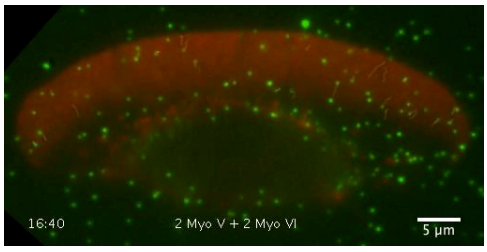

Movie S2 – Scaffolds with 2 myosin V and 2 myosin VI meandering on a keratocyte actin network (red) (Fig. 6A). Scaffolds travel unidirectionally, either towards the cell periphery or the cell center. Data collected at 2 Hz frame rate, 2 mM ATP, RT.

Supplemental Notes S1

Computer aided staple strand sequences for the flat-rectangular DNA origami scaffold (Figs. S3–4)

Core	
r0t11ml1	TTAGATACTATTTTCATTTGGGGAATGCCT
r0t11mr1	TAAGAACGGAGGTTTTGAAGCCTAGTCAGA
r0t11mr2	TAATGCAGTTCGAGCCAGTAATAACTGACCTA
r0t11mr3	AAATCAGAGCTATTTTGCACCCAGAGAATAAC
r0t11mr_fr	ATAAGTCCATATTTAACAACGCCGTGTGAT
r0t11seam_l	AATATCGCTAAGAGGAAGCCCGAAACCTCCCG
r0t11seam_r	CCAGACGACGACAAAAGGTAAAGTATAACCTG
r0t13ml1	GAGTAATGCGGAGACAGTCAAATAACGTTA
r0t13mr1	TAAAGTACCGACAATAAACAACAGGTATTC
r0t13mr2	AATTTAATAAATGCTGATGCAAATTTTTAATG
r0t13mr3	GAGGCATTAACGCGCCTGTTTATCTTCATCGT
r0t13mr_fr	AAATAAGACCTTTTTAACCTCCGTGAGTGA
r0t13seam_l	TTTAGCTAATTTCGCAAATGGTCAAATTCTGT
r0t13seam_r	TATATTTTAGAACGCGAGAAAACTAAAGGGTG
r0t15mr1	CAAGACAAAGTTAATTTCATCTTGAGAATA
r0t15mr3	CTATATGTGGTTTGAAATACCGACCAACATGT
r0t15mr_fr	ATAACCTACAATAACGGATTCGTTATACTT
r0t15seam_l	AGAAAGGCTGTAGGTAAAGATTCATTTTCAAA
r0t17mr3	TCAATTACACATAAATCAATATATGGCTTAGG
r0t19ml1	CCACACAAGGGGTGCCTAATGAGAGCAGGC
r0t19ml3	TCCTGTGTAATTGCGTTGCGCTCAAGAGAGTT
r0t19mr2	CCCTCAATTAACACCGCCTGCAACATTCACCA
r0t19mr_fr	AACAGTTCCACCAGCAGAAGATACATTCTG
r0t19seam_r	AGCATCACGCCAGCAGCAAATGAAATAAAGTG
r0t1ml1	TCCAAAAGTTTCGAGGTGAATTTGTAATGC
r0t1mr2	TTTAACGGGAATGGAAAGCGCAGTCCATCTTT
r0t1seam_r	TTGATGATTCCAGTAAGCGTCATACGGTTTAT
r0t1t_seam	CGCCACCCTCAGAACCGCCACCCTCAGAACCG
r0t1tl1	CCACCCTCAGAGCCACCACCCTCAAAAGGC
r0t1tl2	GGATAGCAAGCCCAATAGGAACCCCAACAGTT
r0t1tl3	TAACACTGAGTTTCGTCACCAGTTTTTCTGT
r0t1tr1	GGTGTATCACCGTACTCAGGAGGTTAATAAGT
r0t21ml1	GAAAATCCCCTTATAAATCAAAACGGCGAA
r0t21ml3	AAGCGGTCGGTTGAGTGTTGTTCCGAGCCCCC
r0t21ml_fl	TTTCCAGTCGTAATCATGGTCACGAAAGGG
r0t21mr2	GTCACACGTTGCAACAGGAAAAACTAAAGGGA
r0t21mr3	GTCAGTATCAATATCTGGTCAGTTGCCCGAAC

r0t21mr_fr	GCCAACATGCTGGTAATATCCAAATCCTGA
r0t21seam_r	AAATGGATTACATTTTGACGCTCACGAAATCG
r0t23b_seam	CGTGGCGAGAAAGGAAGGGAAGAAAATCAGAG
r0t23bl1	GATTTAGAGCTTGACGGGGAAAGCGAATAGCC
r0t23br1	CGGGAGCTAAACAGGAGGCCGATGCTCATG
r0t23br2	TTTTAGACAGGAACGGTACGCCAGGAACAATA
r0t23br3	GAAGTGTTTTTATAATCAGTGAGCTCAAACT
r0t23ml2	CGAGATAGCACGCTGGTTTGCCCCTGAGCTAA
r0t23ml_fl	ACAAGAGCACCGCCTGGCCCTGCTGCCCGC
r0t23mr1	GAAATACCTATTTACATTGGCAGAGTGCCA
r0t23mr3	GCCAGCCAACCAGTAATAAAAGGGAAAACAGA
r0t23seam_l	GCAAAATCTGTTTGATGGTGGTTCATCGTCTG
r0t3ml1	CACTACGAATACACTAAAACACTATCTTGA
r0t3ml2	GCTTGATATTGAAAATCTCCAAAAATTTTCAG
r0t3ml3	GTTTCCATCGATTATACCAAGCGCGACCAGGC
r0t3ml_fl	ACAACCATTGCTAAACAACTTTATGTACCG
r0t3mr1	TTTACCGTACAGGAGTGTACTGGTTAGTAC
r0t3mr2	TCATAATCAATCAAGTTTGCCTTTCAAAAGGG
r0t3mr3	TAAAGCCAGGTCAGTGCCTTGAGTGATATAAG
r0t3mr_fr	ACCGGAATCGATAGCAGCACCGGAAGGTAA
r0t3seam_l	CAGCTTGCGAGCCTTTAATTGTATCATGGCTT
r0t3seam_r	CATAGCCCCGCGTTTTCATCGGCACGAAAGAG
r0t5ml1	CAAGAACCCTGCTCATTCAGTGAAATGCAG
r0t5ml2	ACCCCCAGTAAACGGGTAAAATACCTTAAACA
r0t5ml_fl	GTACAACCTTTGAGGACTAAAGCAATGACA
r0t5mr1	GACTGTAGCCTTATTAGCGTTTGCTCTGAA
r0t5mr2	CGACATTCGAAACGCAAAGACACCATAATAAG
r0t5mr3	AGCGACAGAAAATCACCGGAACCACAAACAAA
r0t5mr_fr	ATATTGAGCAAACGTAGAAAATAGCTATCT
r0t5seam_l	GCAAAAGAAGGCACCAACCTAAAATTTTCGGT
r0t5seam_r	ATATGGTTTTTGTCACAATCAATAAATCAACG
r0t7ml1	ATACATAAAACACTATCATAACCTTGCATC
r0t7mr1	AAGTTTATTACCAGCGCCAAAGAAGCGTCA
r0t7mr2	AGCAAGAATGAACACCCTGAACAATAAATCAA
r0t7mr3	ATATAAAAAACCGATTGAGGGAGGTAATCAGT
r0t7mr_fr	TACCGAAGCAGCCTTTACAGAGCTACAATT
r0t7seam_l	TAACAAAGGGATATTCATTACCCAGAAAATTC
r0t7seam_r	CCACAAGAGAGCGCTAATATCAGAGAGGCATA
r0t9ml1	AAAAAGATGTTTTAATTCGAGCTTTGACCA
r0t9mr1	GGGTAATTATTGAGTTAAGCCCAACGGAAT
r0t9mr2	GATTAGTTTATAGAAGGCTTATCCTGTTCAGC
r0t9mr3	GAATTAACACAATGAAATAGCAATACATACAT

r0t9mr_fr	TTATCCTCAAGCCGTTTTTATTAACAATAG
r0t9seam_l	GTAAGAGCCGCCAAAAGGAATTACGAGATAAC
r0t9seam_r	ACTTGCGGCGAGGCGTTTTAGCGAAGACTTCA
r1t0tr2	GGATAAGTGCCGTCGAGAGGGTTAACAGTGC
r1t0tr3	TAGGATTAGCGGGGTTTTGCTCAGTGCCTATT
r1t10fr1	AGAACAAGGAATCTTACCAACGCTGTCAAAAA
r1t10fr2	TCTTTCCATTAAACCAAGTACCGCATATCCCA
r1t10fr3	AACGGGTAGAGCCTAATTTGCCAAATCCAA
r1t12fr1	AGAATCGCCTGAACAAGAAAAATAACTCATCG
r1t12fr3	TAAAGCCATACGAGCATGTAGAATTCCAAG
r1t14fr1	GAGAGACTGCGTTAAATAAGAATACTTAATTG
r1t14fr2	AATCATAATGAATTTATCAAAATCCGCTATTA
r1t14fr3	GTCAATAGTTACTAGAAAAAGCCACCAGTA
r1t16fr1	CGGGAGAATGCTTCTGTAAATCGTATAGGTCT
r1t16fr2	ATTAATTTATACAGTAACAGTACCCTACCATA
r1t16fr3	AGATGAATTCCCTTAGAATCCTTGAGAAGA
r1t18fr1	CGACAACTATGGAAGGGTTAGAACTTTTACAT
r1t18fr2	TCAAAATTAAGTATTAGACTTTACGGTTATCT
r1t18fr3	GGATTTAGATTTGCACGTAAAACTAACGTC
r1t20fr1	CGAACGAAGAAAGGAATTGAGGAAAAACAATT
r1t20fr2	AAAATATCCTAAAACATCGCCATTGACCTGAA
r1t20fr3	TGATAGCCTTTAGGAGCACTAACCATTTGA
r1t22fr1	ATCGGCCTGAGATAGAACCCTTCTAAAAATAC
r1t22fr2	AGCGTAAGTGCCTGAGTAGAAGAAGCCACCGA
r1t22fr3	ACATCACTAATACGTGGCACAGACGCGAAC
r1t24br4	GTAAAAGAGTCTGTCCATCACGCAGTAATA
r1t2fr1	CAGACGATAACAGTTAATGCCCCCTACCAGGC
r1t2fr2	TCGGAACCCATTGACAGGAGGTTGCGCCACCC
r1t2fr3	GCCGCCAGTATTATTCTGAAACAGAAGGAT
r1t4fr1	TGAAACCACCGCCTCCCTCAGAGCAGGCAGGT
r1t4fr2	TCAGAACCTAGCAAGGCCGGAAACAAGGTGAA
r1t4fr3	ATTACCATGCCACCCTCAGAGCCCAGAGCC
r1t6fr1	GTATGTTACGGAAATTATTCATTAGTCACCAA
r1t6fr2	TTATCACCATGATTAAGACTCCTTGTAAGCAG
r1t6fr3	GAACTGGCGTCACCGACTTGAGCTAGCACC
r1t8fr1	TGAAAATAGCCCTTTTTAAGAAAAATTACGCA
r1t8fr2	ATAGCCGACGATTTTTTGTTTAACAACGAGCG
r1t8fr3	ATAAGAAAACAAAGTTACCAGAACCCAAAA
r-1t0tl4	CAACGCCTGTAGCATTCCACAGATTTGTCG
r-1t10fl1	AAACGAGAGAGTACCTTTAATTGCTACGGTGT
r-1t10fl2	ATAAGAGGCTCAAATGCTTTAAACAGAGGGGG
r-1t10fl3	GAATCCCCTCATTTTTGCGGATGAGCTCAA

r-1t12fl2	GGCAAAGAAAATATGCAACTAAAGTCCTTTTG
r-1t12fl3	CATGTTTTATTAGCAAAATTAAGTTGTACC
r-1t14fl1	GAGAAGCCGAGAGGGTAGCTATTTCATATGTA
r-1t14fl2	TCTACAAATATGACCCTGTAATACACAGGCAA
r-1t14fl3	AAAAACATGGCTATCAGGTCATTTGAACGG
r-1t16fl1	CCCCGGTTGCTTTCATCAACATTACGTAACCG
r-1t16fl2	CGAGTAACAAACTAGCATGTCAATTTGAGAGA
r-1t16fl3	TAATCGTAAACCCGTCGGATTCTGGATAGG
r-1t18fl1	TGCATCTGCTGCAAGGCGATTAAGGGTACCGA
r-1t18fl2	CGCCAGGGGTGTAGATGGGCGCATAATGTGAG
r-1t18fl3	TCACGTTGTTTTCCCAGTCACGAATGCCTG
r-1t20fl1	GCTCGAATTCGGGAAACCTGTCGTACAGCTGA
r-1t20fl2	CATTAATGCTCTAGAGGATCCCCGTTGGGTAA
r-1t20fl3	CAGGTCGAAATCGGCCAACGCGCGTGGTTT
r-1t22fl1	TTGCCCTTTCCACTATTAAAGAACGCCGTAAA
r-1t22fl2	CAACGTCAACCAGTGAGACGGGCAGCCAGCTG
r-1t22fl3	TTCTTTTCAAGGGCGAAAAACCGTCACCCA
r-1t24bl2	GCACTAAATCGGAACCCTAAAGGAGTTTGGA
r-1t24bl3	AATCAAGTTTTTTGGGGTCGAGGTGTGGACTC
r-1t2fl1	ATGGGATTTCGCCCACGCATAACCGCAACGGC
r-1t2fl2	CGGTCGCTGACGTTAGTAAATGAAACAAACTA
r-1t2fl3	TCTTTCCAGAGGCTTGCAGGGAGAGCAGCG
r-1t4fl1	TACAGAGGGGAGATTTGTATCATCACTTTGAA
r-1t4fl2	AATTGTGTCATCGGAACGAGGGTAGATATATT
r-1t4fl3	AAAGACAGCGAAATCCGCGACCTACGGTCA
r-1t6fl1	AGAGGACACTTGAGATGGTTTAATAACGAACT
r-1t6fl2	TAATCATTGGAACCGAACTGACCAGCCTGATA
r-1t6fl3	ATCATAAGGTGAATTACCTTATGGGACGTT
r-1t8fl1	AACGGAACCAAAAGAAGTTTTGCCAGTTCAGA
r-1t8fl2	TAATAGTAAAATCTACGTTAATAATTCAACTT
r-1t8fl3	GGGAAGAAAAATGTTTAGACTGGATTCATT
rt-rem1	AGCACGTATAACGTGCTTTCCTCGTTAG
rt-rem2	ACAGGGCGCGTACTATGGTTGCTTTGACG
rt-rem3	ACCACACCCGCCGCGCTTAATGCGCCGCT
rt-rem4	CAAGTGTAGCGGTCACGCTGCGCGTAACC
rt-rem5	AGCGAAAGGAGCGGGCGCTAGGGCGCTGG

Edge staples that binds to Cy3-labeled oligo3 (complementary sequence to oligo3 in lowercase)

oligo3-TT-Cy3	agctgcaggctcgacctgcgTT/3Cy3Sp/
r1t0_edge_r_2_RC_oligo3	TTTTTTTAGACTCCTCAAGATGAAAGTATTAAGcgcaggtcgagcctgcagct
r1t2_edge_r_2 _RC_oligo3	TTTTTTTCCAGAACCACCACACCACCCTCAGAGcgcaggtcgagcctgcagct
r1t4_edge_r_2 _RC_oligo3	TTTTTTTGCAAAATCACCAGCATTTGGGAATTAcgcaggtcgagcctgcagct

r1t6_edge_r_2 _RC_oligo3	TTTTTTTTAATAACGGAATAGGAAACCGAGGAAcgcaggtcgagcctgcagct
r1t8_edge_r_2 _RC_oligo3	TTTTTTTTATTATTTATCCCGTTACAAAATAAAcgcaggtcgagcctgcagct
r1t10_edge_r_2_RC_oligo3	TTTTTTTTCTTTCCTTATCAACCAATCAATAATcgcaggtcgagcctgcagct
r1t12_edge_r_2_RC_oligo3	TTTTTTTTATACAAATTCTTTGTTTAGTATCATcgcaggtcgagcctgcagct
r1t14_edge_r_2_RC_oligo3	TTTTTTTAGATTAAGACGCTGAAAACATAGCGAcgcaggtcgagcctgcagct
r1t16_edge_r_2_RC_oligo3	TTTTTTTAGATTTTCAGGTTAGAAATAAAGAAAcgcaggtcgagcctgcagct
r1t18_edge_r_2_RC_oligo3	TTTTTTTTCAATAGATAATAAACTAATAGATTAcgcaggtcgagcctgcagct
r1t20_edge_r_2_RC_oligo3	TTTTTTTTTAGTCTTTAATGCAATATTTTTGAAcgcaggtcgagcctgcagct
r1t22_edge_r_2_RC_oligo3	TTTTTTTTACTTCTTTGATTAAATTAACCGTTGcgcaggtcgagcctgcagct
r---1t2_edge_l_2_RC_oligo3	TTTTTTTAACGATCTAAAGTCAGCCCTCATAGTcgcaggtcgagcctgcagct
r---1t4_edge_l_2_RC_oligo3	TTTTTTTGATCGTCACCCTCTTAAAGGCCGCTTcgcaggtcgagcctgcagct
r---1t6_edge_l_2_RC_oligo3	TTTTTTTGAACGAGGCGCAGGCTCCATGTTACTcgcaggtcgagcctgcagct
r---1t8_edge_l_2_RC_oligo3	TTTTTTTATTATACCAGTCACGATTTTAAGAACcgcaggtcgagcctgcagct
r---1t10_edge_l_2_RC_oligo3	TTTTTTTAATCGTCATAAATATAGCGTCCAATAcgcaggtcgagcctgcagct
r---1t12_edge_l_2_RC_oligo3	TTTTTTTAATATAATGCTGTGCTTAGAGCTTAAcgcaggtcgagcctgcagct
r---1t14_edge_l_2_RC_oligo3	TTTTTTTAAAGCTAAATCGGCAATAAAGCCTCA cgcaggtcgagcctgcagct
r---1t16_edge_l_2_RC_oligo3	TTTTTTTACAAGAGAATCGAGCCTGAGAGTCTGcgcaggtcgagcctgcagct
r---1t18_edge_l_2_RC_oligo3	TTTTTTTATTGACCGTAATGCCGTGGGAACAAAcgcaggtcgagcctgcagct
r---1t20_edge_l_2_RC_oligo3	TTTTTTTGTGCCAAGCTTGCCGTTGTAAAACGAcgcaggtcgagcctgcagct
r---1t22_edge_l_2_RC_oligo3	TTTTTTTATTGGGCGCCAGGGGGGAGAGGCGGTcgcaggtcgagcctgcagct
r---1t24_edge_l_2_RC_oligo3	TTTTTTTACTACGTGAACCATCTATCAGGGCGAcgcaggtcgagcctgcagct

Core staples that bind to oligo1-myosin VI

BG-oligo1	TTTTTTgatacgcgccaatctctata
r0t1mr_fr-TR-oligo1	CCGTATATGGCCTTGATATTCAGAGCCACCtatagagattggcgcgtatc
r1t12fr2-MR-oligo1	tatagagattggcgcgtatcTCCTAATTACGCTCAACAGTAGGGAACACCGG
r0t17mr_fr-BR-oligo1	CTGAATACGTATTAAATCCTTTGGCAAATCtatagagattggcgcgtatc
r0t17ml3_hp_org-BL-oligo1	CAGCTTTCCTATTACGCCAGCTGGTAGCTGTTtatagagattggcgcgtatc
r-1t12fl1-ML-oligo1	tatagagattggcgcgtatcCTGGAAGTACATCCAATAAATCATTTTTGCGG
r0t1ml3-TL-oligo1	TTTTCACGCCGATAGTTGCGCCGAACTTTTTCtatagagattggcgcgtatc

Core staples that bind to oligo2-myosin V

BG-oligo2	TTTTTTatgaacttgcgctcaattcc
r0t1mr_fr-TR-oligo1	CCGTATATGGCCTTGATATTCAGAGCCACCggaattgagcgcaagttcat
r1t12fr2-MR-oligo1	ggaattgagcgcaagttcatTCCTAATTACGCTCAACAGTAGGGAACACCGG
r0t17mr_fr-BR-oligo1	CTGAATACGTATTAAATCCTTTGGCAAATCggaattgagcgcaagttcat
r0t17ml3_hp_org-BL-oligo1	CAGCTTTCCTATTACGCCAGCTGGTAGCTGTTggaattgagcgcaagttcat
r-1t12fl1-ML-oligo1	ggaattgagcgcaagttcatCTGGAAGTACATCCAATAAATCATTTTTGCGG
r0t1ml3-TL-oligo1	TTTTCACGCCGATAGTTGCGCCGAACTTTTTCggaattgagcgcaagttcat

Core staples that does not to either oligo 1 nor oligo2 (control)

r0t1mr_fr-TR	CCGTATATGGCCTTGATATTCAGAGCCACC
r1t12fr2-MR	TCCTAATTACGCTCAACAGTAGGGAACACCGG
r0t17mr_fr-BR	CTGAATACGTATTAAATCCTTTGGCAAATC
r0t17ml3_hp_org-BL	CAGCTTTCCTATTACGCCAGCTGGTAGCTGTT
r-1t12fl1-ML	CTGGAAGTACATCCAATAAATCATTTTTGCGG
r0t1ml3-TL	TTTTCACGCCGATAGTTGCGCCGAACTTTTTC

Purification strands

spacer-strand	CGATGGATGACTGACTGATGGATGACTTAAATTGACTATGACTATGATACTGACTGATTACG
biotin-strand	CATCCATCAGTCAGTCATCCATCGTTTTTTT-biotin
origami-strand (r1t0)	TTTTTTTAGACTCCTCAAGATGAAAGTATTAAGTTGGATAGTCAGTATCATAGTCATAGTCAA
elution-strand	CGTAATCAGTCAGTATCATAGTCATAGTCAATTTAAGTCATCCATCAGTCAGTCATCCATCG

Strands for gliding assay

Biotin-Oligo1-C1	biotin-TTTTTTtatagagattggcgcgtatc
Biotin-Oligo1-C1	biotin-TTTTTTggaattgagcgcaagttcat

Supplemental Table S1 – Statistics

Numbers of trajectories analyzed for indicated experimental conditions. Experimental data were collected on at least four different keratocytes. The minimum number of detected trajectories was 112 and on average 852. End-to-end speed and shape factor analyses were restricted to long trajectories (RL ≥ 1 μm; N ≥ 58).

Experiments	**N** (trajectories)	
	All trajectories	Long trajectories; RL≥ 1.000 μm
Myosin V (– scaffold)	791	168
Myosin VI (– scaffold)	1181	203
DNA scaffold + 1 myosin V	413	71
DNA scaffold + 2 myosin V	1688	501
DNA scaffold + 3 myosin V	895	208
DNA scaffold + 4 myosin V	385	191
DNA scaffold + 5 myosin V	776	240
DNA scaffold + 6 myosin V	1398	338
DNA scaffold + 1 myosin VI	317	64
DNA scaffold + 2 myosin VI	1897	636
DNA scaffold + 3 myosin VI	205	86
DNA scaffold + 4 myosin VI	112	58
DNA scaffold + 5 myosin VI	687	437

DNA scaffold + 6 myosin VI	1185	617
DNA scaffold + 6 myosin V/VI	452	391
DNA scaffold + 6 myosin VI/V	569	492
DNA scaffold + 1 myosin V + 1 myosin VI	828	425
DNA scaffold + 2 myosin V + 2 myosin VI	1837	546